ISSN 1726-5749

# SENSORS & TRANSDUCERS

vol. 76
2/07


## Chemical Sensors and Biosensors

International Frequency Sensor Association Publishing

IFSA

# Sensors & Transducers

Volume 76
Issue 2
February 2007

www.sensorsportal.com

ISSN 1726-5479

Sensors & Transducers Journal (ISSN 1726-5479) is a peer review international journal published monthly online by International Frequency Sensor Association (IFSA). Available in electronic and CD-ROM. 

Sensors & Transducers Journal

# Contents

Volume 76
Issue 2
February 2007

www.sensorsportal.com

ISSN 1726-5479

## Research Articles



## Short Communication



Authors are encouraged to submit article in MS Word (doc) and Acrobat (pdf) formats by e-mail: editor@sensorsportal.com
Please visit journal's webpage with preparation instructions: http://www.sensorsportal.com/HTML/DIGEST/Submition.htm

*Sensors & Transducers Journal, Vol.76, Issue 2, February* **2007,** *pp.945-968*

www.sensorsportal.com

**Sensors & Transducers**

**ISSN 1726-5479**

*http://www.sensorsportal.com*

# Advances in Biosensing Methods

**Reema Taneja, Kennon C. Shelton, Raymond Carlisle**
**Ajit Sadana**
Chemical Engineering Department
University of Mississippi
University, MS 38677-1848, USA
Phone: (662) 915-5349, fax: (662) 915-7023,
E-mail: cmsadana@olemiss.edu

*Received: 31 January 2006 / Accepted: 22 February 2007 / Published: 26 February 2007*

**Abstract:** A fractal analysis is presented for the binding and dissociation (if applicable) kinetics of analyte-receptor reactions occurring on biosensor surfaces. The applications of the biosensors have appeared in the recent literature. The examples provided together provide the reader with a perspective of the advances in biosensors that are being used to detect analytes of interest. This should also stimulate interest in applying biosensors to other areas of application.

The fractal analysis limits the evaluation of the rate constants for binding and dissociation (if applicable) for the analyte-receptor reactions occurring in biosensor surfaces. The fractal dimension provides a quantitative measure of the degree of heterogeneity on the biosensor surface. Predictive relations are presented that relate the binding co-efficient with the degree of heterogeneity or the fractal dimension on the biosensor surface.

**Keywords**: Biosensors, advances, fractal kinetics, binding, dissociation

## 1. Introduction

Biosensors have received increasing attention as a means of detecting different types of analytes in different arenas such as bioterrorism and in the early detection of the emergence and proliferation of different types of diseases. Though some techniques such as ELISA and the surface plasmon resonance (SPR) biosensor techniques have gained considerable attention recently, needless to say these detection techniques are not perfect and do have flaws which need to be improved upon. For example, ELISA is time-sensitive, and the surface plasmon resonance (SPR) technique does involve

the presence of diffusional limitations and heterogeneities, for example, of the receptors on the biosensor surface. Also, on using the ELISA technique [1], indicate that for the detection of human IgG, nineteen hours are required from analyte immobilization to binding confirmation by chromophore detection. Some of the drawbacks may be minimized by appropriate handling and experimental procedures. Nevertheless, as with all techniques there is room for improvement in these techniques themselves or in the development of other novel biosensing techniques. Some of the novel techniques to be presented in this manuscript may be in their infancy, but they do exhibit potential as a useful detection technique. Modifications in the standard SPR biosensor technique, as an example, are also presented. The biosensor techniques to be presented in this manuscript may be taken as only model examples. In no way are we indicating that these are in any way representative of all other biosensor techniques recently developed or in the process of development.

In this manuscript, we present a fractal analysis of (a) the binding of different concentrations of mouse monoclonal anti-rabbit IgG in solution to rabbit patterned cells using a diffraction-based sandwich immunoassay [2], (b) the binding and hybridization of DNA using a double-wavelength technique for surface plasmon resonance measurements [3], (c) binding and dissociation of different concentrations of GSH (Glutathione)-MPC (monolayer protected clusters) in solution to polyclonal antibody plus protein A immobilized on a quartz crystal microbalance (QCM) [4], and the (d) binding and dissociation of substance P (neuropeptide) (SP) in solution to quencher-labeled mAb (monoclonal antibody) SP31 using the SPIT-FRI (solid-phase immobilized tripod for fluorescent renewable immunoassay) procedure [5]. Binding and dissociation rate coefficients and affinity values are provided where ever possible. Fractal dimension values for the binding and the dissociation phases are also given. It should be pointed out that the fractal analysis is one possible way to analyze the binding and the dissociation kinetics present in these types of analyte-receptor biosensor systems. The fractal analysis method does, however, include the involvement of external diffusional limitations and the presence of heterogeneities present in these types of analyte-receptor biosensor systems.

## 2. Theory

Havlin [6] has reviewed and analyzed the diffusion of reactants towards fractal surfaces. The details of the theory and the equations involved for the binding and the dissociation phases for analyte-receptor binding are available [7]. The details are not repeated here; except that just the equations are given to permit an easier reading. These equations have been applied to other biosensor systems [8]. For most applications, a single- or a dual-fractal analysis is often adequate to describe the binding and the dissociation kinetics. Peculiarities in the values of the binding and the dissociation rate coefficients, as well as in the values of the fractal dimensions with regard to the dilute analyte systems being analyzed will be carefully noted, if applicable.

### 2.1 Single-fractal analysis

#### *2.1.1 Binding rate coefficient.*

Havlin [6] indicates that the diffusion of a particle (analyte [Ag]) from a homogeneous solution to a solid surface (e.g. receptor [Ab]-coated surface) on which it reacts to form a product (analyte-receptor complex; (Ab.Ag)) is given by:

$$(\text{Analyte.Receptor}) \sim \begin{cases} t^{(3-D_{f,bind})/2} = t^{p} & (t < t_c) \\ t^{1/2} & (t > t_c) \end{cases} \quad (1a)$$

Here $D_{f,bind}$ or $D_f$ (used later on in the manuscript) is the fractal dimension of the surface during the binding step. The $t_c$ is the cross-over value. Havlin [6] indicates that the cross-over value may be determined by $r_c^2 \sim t_c$ . Above the characteristic length, $r_c$, the self-similarity of the surface is lost and the surface may be considered homogeneous. Above time $t_c$, the surface may be considered homogeneous since the self-similarity property disappears and 'regular' diffusion is now present. For a homogeneous surface where $D_f$ is equal to 2, and when only diffusional limitations are present, $p = ½$ as it should be. Another way of looking at the $p = ½$ case (where $D_{f,bind}$ is equal to two) is that the analyte in solution views the fractal object, in our case, the receptor-coated biosensor surface, from a 'large distance.' In essence, in the association process, the diffusion of the analyte from the solution to the receptor surface creates a depletion layer of width $(Đt)^{½}$ where Đ is the diffusion constant. This gives rise to the fractal power law, (Analyte.Receptor) $\sim t^{(3 - D_{f,bind})/2}$. For the present analysis, $t_c$ is arbitrarily chosen and we assume that the value of $t_c$ is not reached. One may consider the approach as an intermediate 'heuristic' approach that may be used in the future to develop an autonomous (and not time-dependent) model for diffusion-controlled kinetics.

### *2.1.2 Dissociation rate coefficient.*

The diffusion of the dissociated particle (receptor [Ab] or analyte [Ag]) from the solid surface (e.g., analyte [Ag]-receptor [Ab]) complex coated surface) into solution may be given, as a first approximation by:

$$(\text{Ab.Ag}) \approx -t^{(3-D_{f,diss})/2} = t^{p} \quad (t > t_{diss}) \quad (1b)$$

Henceforth, its concentration only decreases. The dissociation kinetics may be analyzed in a manner 'similar' to the binding kinetics.

## 2.2 Dual-fractal analysis

### *2.2.1 Binding rate coefficient.*

Sometimes the binding curve exhibits complexities and two parameters (k, $D_f$ ) are not sufficient to adequately describe the binding kinetics. This is further corroborated by low values of $r^2$ factor (goodness-of-fit). In that case, one resorts to a dual-fractal analysis (four parameters; $k_1$, $k_2$, $D_{f1}$, and $D_{f2}$) to adequately describe the binding kinetics. The single-fractal analysis presented above is thus extended to include two fractal dimensions. At present, the time ($t = t_1$) at which the 'first' fractal dimension 'changes' to the 'second' fractal dimension is arbitrary and empirical. For the most part, it is dictated by the data analyzed and experience gained by handling a single-fractal analysis. A smoother curve is obtained in the 'transition' region, if care is taken to select the correct number of points for the two regions. In this case, the product (antibody-antigen; or analyte-receptor complex, Ab.Ag or analyte.receptor) is given by:

$$(Ab.Ag) \approx \begin{cases} t^{(3-D_{f1,bind})/2} = t^{p1} & (t < t_1) \\ t^{(3-D_{f2,bind})/2} = t^{p2} & (t_1 < t < t_2) = t_c \\ t^{1/2} & (t > t_c) \end{cases} \quad (1c)$$

In some cases, as mentioned above, a triple-fractal analysis with six parameters ($k_1$, $k_2$, $k_3$, $D_{f1}$, $D_{f2}$, and $D_{f3}$) may be required to adequately model the binding kinetics. This is when the binding curve exhibits convolutions and complexities in its shape, perhaps due to the very dilute nature of the analyte (in some of the cases to be presented) or for some other reasons. Also, in some cases, a dual-fractal analysis may be required to describe the dissociation kinetics.

## 3. Results

At the outset, it is appropriate to indicate that a fractal analysis will be applied to the data obtained for analyte-receptor binding and dissociation (if applicable) data for different types of either novel biosensor systems or biosensor systems with significant modifications. This is one possible explanation for analyzing the diffusion-limited binding and dissociation kinetics assumed to be present in all of the systems analyzed. The parameters thus obtained would provide a useful comparison of different situations. Alternate expressions involving saturation, first-order reaction, and no diffusion limitations are possible, but they are apparently deficient in describing the heterogeneity that inherently exists on the surface. The analyte-receptor binding as well as the dissociation reaction is a complex reaction and the fractal analysis via the fractal dimension and the rate coefficient for binding or dissociation provide a useful lumped parameter(s) analysis of the diffusion-limited situation.

Also, we do not present any independent proof or physical evidence for the existence of fractals in the analysis of these analyte-receptor binding/dissociation systems except by indicating that it has been applied in other areas and that it is a convenient means of making more quantitative the degree of heterogeneity that exists on the surface. Thus, in all fairness, this is one possible way by which to analyze this analyte-receptor binding/dissociation data for novel biosensor systems. One might justifiably argue that appropriate modeling may be achieved by using a Langmuirian or other approach. The Langmuirian approach has a major drawback because it does not allow for or accommodate the heterogeneity that exists on the surface.

The Langmuir approach was originally developed for gases [9]. Researchers in the past have successfully modeled the adsorption behavior of analytes in solution to a solid surface using the Langmuir model even though it does not conform to theory. Rudzinski et al.[10] indicate that other appropriate "liquid" counterparts of the empirical isotherms have been developed. These include counterparts of the Freundlich [11], Dubinin-Radushkevich [12], and Toth [13] empirical equations. These studies with their known constraints have provided some "restricted" physical insights into the adsorption of adsorbates on different surfaces. The Langmuir approach may be used to model the data presented if one assumes the presence of discrete classes of sites (for example, double exponential analysis as compared to a single exponential analysis). Lee and Lee [14] indicate that the fractal approach has been applied to surface science, for example, adsorption and reaction processes. These authors emphasize that the fractal approach provides a convenient means of representing the different structures and morphology at the reaction surface. These authors also emphasize the use of the fractal approach as a predictive approach and a means to develop optimal structures.

Goh et al. [8] indicate that diffraction-based sensing may be used to analyze interactions between two or more molecules. In order to ensure that one may obtain kinetic and equilibrium rate coefficients, these authors emphasize that specific molecular interactions may be continuously monitored by observing intensity changes of the diffraction image from a patterned substrate. They further indicate that diffraction-based sensing has been used as a diagnostic tool to assay pH [15] small molecules [16,17], proteins [8,17], and whole cells [18,19].In spite of the disadvantages of using secondary labels such as high cost and longer sample preparation time, Goh et al. [8] have used diffraction-based sensing through the use of a secondary label to reduce the limit of detection of the detection of anti-rabbit IgG by a factor of forty on using a gold-conjugated secondary antibody.

Fig.1a shows the binding of 25 ng/mL mouse monoclonal anti-rabbit IgG in solution to rabbit IgG patterned cells [8]. A single-fractal analysis is adequate to describe the binding kinetics. Table 1 shows the values of the binding rate coefficient k and the fractal dimension $D_f$ obtained using Corel Quattro Pro [20] to fit the data. Equation 1a was used to fit the data, and the equation was used to obtain the value of k and $D_f$ for a single-fractal analysis. The values of the parameters presented in Table 1 are within 95 % confidence limits. For example, for the binding of 25 ng/mL mouse monoclonal anti-rabbit IgG in solution to rabbit IgG patterned cells, the binding rate coefficient, k for a single-fractal analysis reported is 5.8179 ± 0.0540. The 95 % confidence limit indicates that 95 % of the k values will lie between 5.7639 and 5.8179. This indicates that the values are precise and significant.

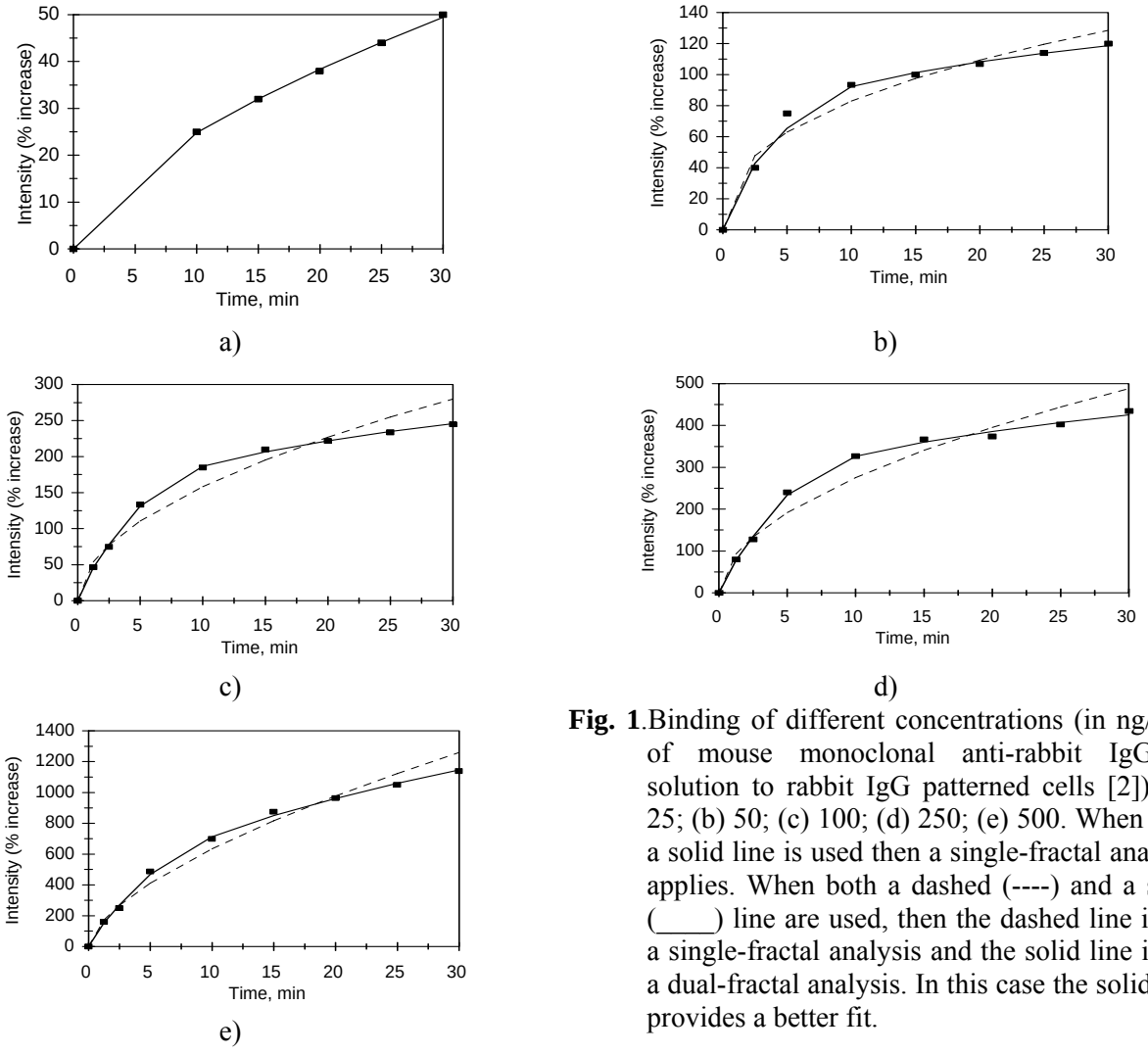


**Fig. 1**.Binding of different concentrations (in ng/mL) of mouse monoclonal anti-rabbit IgG in solution to rabbit IgG patterned cells [2]): (a) 25; (b) 50; (c) 100; (d) 250; (e) 500. When only a solid line is used then a single-fractal analysis applies. When both a dashed (----) and a solid (____) line are used, then the dashed line is for a single-fractal analysis and the solid line is for a dual-fractal analysis. In this case the solid line provides a better fit.

**Table 1.** Binding rate coefficients and fractal dimensions for (a) the binding of different concentrations of mouse monoclonal anti-rabbit IgG in solution to rabbit IgG patterned cells, and (b) binding of different 5 μg/mL monoclonal anti-rabbit IgG in solution to rabbit IgG patterned cells, and (c) followed by 1 and 5 μg/mL anti-mouse gold conjugate [2].

| Mouse monoclonal anti-rabbit IgG in solution (ng/mL)/rabbit IgG patterned cells | **k** | **$k_1$** | **$k_2$** | **$D_f$** | **$D_{f1}$** | **$D_{f2}$** |
|---|---|---|---|---|---|---|
| (a) 25 | 5.8719 ±0.0540 | na | na | 1.7464 ±0.0212 | na | na |
| 50 | 33.1758 ±4.6043 | 24.4270 ±4.4288 | 54.5952 ±0.7562 | 2.2032 ±0.1169 | 1.7750 ±0.3398 | 2.5434 ±0.03172 |
| 100 | 48.0623 ±7.0313 | 38.7559 ±1.6747 | 105.0776 ±1.1673 | 1.9638 ±0.08964 | 1.4836 ±0.08630 | 2.5004 ±0.02548 |
| 250 | 83.0593 ±13.5538 | 65.2400 ±4.4233 | 187.3647 ±4.8296 | 1.9578 ±0.09924 | 1.4122 ±0.1338 | 2.5176 ±0.05868 |
| 500 | 151.3012 ±16.990 | na | na | 1.7542 ±0.06986 | na | na |
| (b) 5 μg/mL monoclonal anti-rabbit in solution/rabbit IgG patterned cells | 19.7865 ±1.7548 | na | na | 2.2290 ±0.06618 | na | na |
| Mouse monoclonal anti-rabbit IgG in solution (ng/mL)/rabbit IgG patterned cells | **k** | **$k_1$** | **$k_2$** | **$D_f$** | **$D_{f1}$** | **$D_{f2}$** |
| (c ) 1 μg/mL anti-mouse gold conjugate/rabbit IgG patterned cells | 21.4603 ±2.2370 | 17.5609 ±1.3825 | 32.2395 ±2.2430 | 1.4368 ±0.0821 | 1.1494 ±0.2212 | 1.7336 ±0.10898 |
| 5 μg/mL anti-mouse gold conjugate/rabbit IgG patterned cells | 60.0433 ±11.0704 | 31.0439 ±3.8759 | 149.086 ±6.881 | 1.7206 ±0.1349 | 0.5810 ±0.4778 | 2.3736 ±0.1055 |

Fig.1b shows the binding of 50 ng/mL mouse monoclonal anti-rabbit IgG in solution to rabbit IgG patterned cells [8]. In this case a dual-fractal analysis is required to adequately describe the binding kinetics. The values of (a) the binding rate coefficient, k and the fractal dimension, $D_f$ for a single-fractal analysis and (b) the binding rate coefficients, $k_1$ and $k_2$, and the fractal dimensions, $D_{f1}$ and $D_{f2}$ for a dual-fractal analysis are given in Table 1. It is of interest to note that as the fractal dimension (or the degree of heterogeneity on the surface) increases by 43.3 % from a value of $D_{f1}$ equal to 1.7750 to $D_{f2}$ equal to 2.5434, the binding rate coefficient increases by a factor of 2.24 from a value of $k_1$ equal to 24.427 to $k_2$ equal to 54.595. In this case too, an increase in the degree of heterogeneity leads to an increase in the binding rate coefficient.

Fig.1c shows the binding of 100 ng/mL mouse monoclonal anti-rabbit IgG in solution to rabbit IgG patterned cells [8]. In this case a dual-fractal analysis is required to adequately describe the binding

kinetics. The values of (a) the binding rate coefficient k and the fractal dimension, $D_f$ for a single-fractal analysis, and (b) the binding rate coefficients, $k_1$ and $k_2$, and the fractal dimensions, $D_{f1}$ and $D_{f2}$ for a dual-fractal analysis are given in Table 1. It is of interest to note that as the fractal dimension (or the degree of heterogeneity on the surface) increases by 68.5 % from a value of $D_{f1}$ equal to 1.4836 to $D_{f2}$ equal to 2.5004, the binding rate coefficient increases by a factor of 2.71 from a value of $k_1$ equal to 38.7559 to $k_2$ equal to 105.0776. Once again, an increase in the degree of heterogeneity leads to an increase in the binding rate coefficient. Also, note that an increase in the mouse monoclonal anti-rabbit IgG in solution by a factor of two from 50 to 100 ng/mL in soluton leads to an increase in (a) the binding rate coefficient, $k_1$ by a factor of 1.587 from a value of 24.427 to 38.756 and in (b) the binding rate coefficient $k_2$ by a factor of 1.924 from a value of 54.5952 to 105.0776.

Fig.1d shows the binding of 250 ng/mL mouse monoclonal anti-rabbit IgG in solution to rabbit IgG patterned cells [8]. In this case a dual-fractal analysis is required to adequately describe the binding kinetics. The values of (a) the binding rate coefficient, k and the fractal dimension, $D_f$ for a single-fractal analysis, and (b) the binding rate coefficients, $k_1$ and $k_2$, and the fractal dimensions, $D_{f1}$ and $D_{f2}$ for a dual-fractal analysis are given in Table 1.

Fig.1e shows the binding of 500 ng/mL mouse monoclonal anti-rabbit IgG in solution to rabbit IgG patterned cells [8]. In this case a dual-fractal analysis is required to adequately describe the binding kinetics. The values of (a) the binding rate coefficient, k and the fractal dimension, $D_f$ for a single-fractal analysis, and (b) the binding rate coefficients, $k_1$ and $k_2$, and the fractal dimensions, $D_{f1}$ and $D_{f2}$ for a dual-fractal analysis are given in Table 1.

In both of the cases presented in Fig.1d and 1e, the trends are similar to the ones observed in Fig. 1b and 1c. They are not repeated here to avoid repetition. For a dual-fractal analysis, Table 1 and Fig. 2a indicate the increase in the binding rate coefficient, $k_1$ with an increase in the anti-rabbit IgG concentration in solution. In the 50-250 ng/mL anti-rabbit IgG concentration in solution the binding rate coefficient, $k_1$ is given by:

$$k_1 = (2.2955 \pm 0.0731)\,[\text{anti-rabbit IgG}]^{0.6082 \pm 0.0274} \tag{2a}$$

The fit is good. Only three data points are available. The availability of more data points would lead to a more reliable fit. The binding rate coefficient, $k_1$ is only mildly sensitive to the anti-rabbit IgG concentration in solution as noted by the 0.6082 order of dependence exhibited. The non-integer order of dependence exhibited lends support to the fractal nature of the system.

For a dual-fractal analysis, Table 1 and Fig.2b indicate the decrease in the fractal dimension, $D_{f1}$ with an increase in the anti-rabbit IgG concentration in solution. In the 50-250 ng/mL anti-rabbit IgG concentration in solution the fractal dimension, $D_{f1}$ is given by:

$$D_{f1} = (2.9477 \pm 0.2005)\,[\text{anti-rabbit IgG}]^{-0.1375 \pm 0.05764} \tag{2b}$$

The fit is reasonable. Only three data points are available. The availability of more data points would lead to a more reliable fit. The fractal dimension $D_{f1,}$ is only very slightly sensitive to the anti-rabbit IgG concentration in solution as noted by the negative 0.1375 order of dependence exhibited. It should be pointed out that the fractal dimension is based on a log scale and that even small changes in the fractal dimension exhibited indicate significant changes in the degree of heterogeneity on the sensing surface.

For a dual-fractal analysis, Table 1 and Fig.2c indicate the decrease in the binding rate coefficient $k_1$ with an increase in the fractal dimension, $D_{f1}$. In the 50-250 ng/mL anti-rabbit IgG concentration in solution the binding rate coefficient, $k_1$ is given by:

$$k_1 = (211.801 \pm 57.348)\, D_{f1}^{-3.8434 \pm 1.4081} \quad (2c)$$

The fit is good. Only three data points are available. The availability of more data points would lead to a more reliable fit. The binding rate coefficient, $k_1$ is very sensitive to the fractal dimension, $D_{f1}$ or the degree of heterogeneity that exists on the surface as noted by the negative 3.8434 order of dependence exhibited.

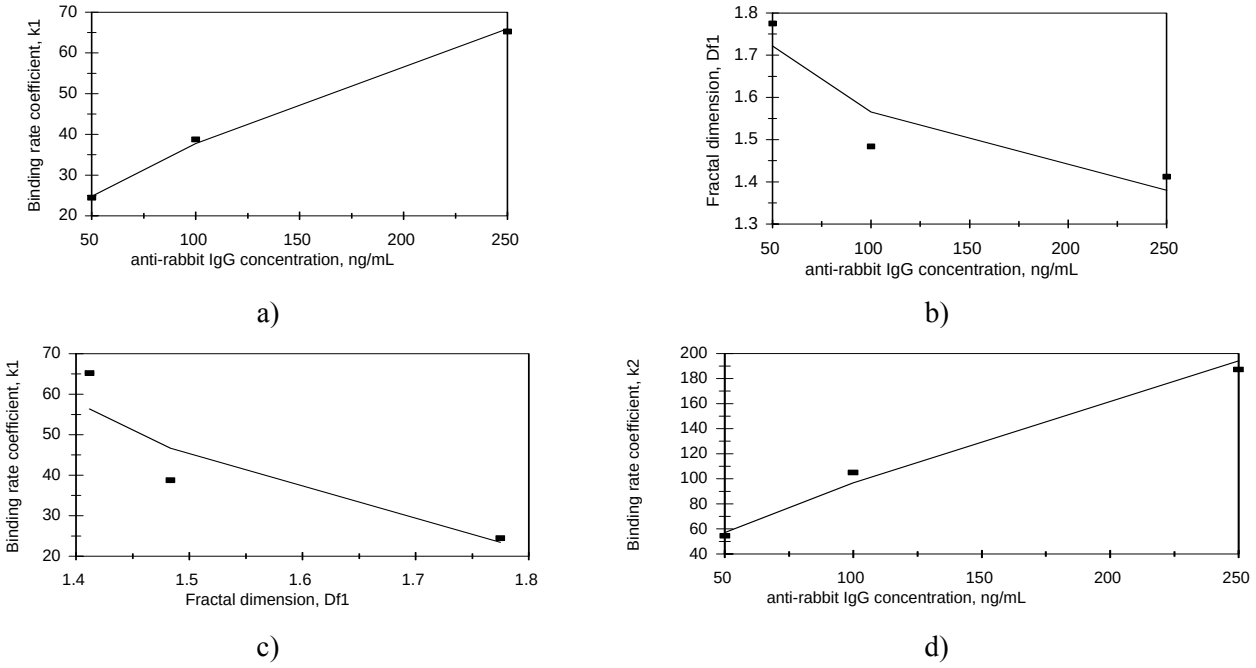


**Fig. 2.** (a) Increase in the binding rate coefficient, $k_1$ with an increase in the anti-rabbit IgG concentration (in ng/mL) in solution; (b) Decrease in the fractal dimension, Df1 with an increase in the anti-rabbit IgG concentration (in ng/mL) in solution; (c) Decrease in the binding rate coefficient, $k_1$ with an increase in the fractal dimension, $D_{f1}$; (d) Increase in the binding rate coefficient, $k_2$ with an increase in the anti-rabbit IgG concentration (in ng/mL) in solution.

For a dual-fractal analysis, Table 1 and Fig.2d indicate the increase in the binding rate coefficient, $k_2$ with an increase in the anti-rabbit IgG concentration in solution. In the 50-250 ng/mL anti-rabbit IgG concentration in solution the binding rate coefficient, $k_2$ is given by:

$$k_2 = (2.9356 \pm 0.3109)\, [\text{anti-rabbit IgG}]^{0.7591 \pm 0.08817} \quad (2d)$$

The fit is good. Only three data points are available. The availability of more data points would lead to a more reliable fit. The binding rate coefficient, $k_1$ is only mildly sensitive to the anti-rabbit IgG concentration in solution as noted by the 0.7591 order of dependence exhibited. The non-integer order of dependence exhibited lends support to the fractal nature of the system. The binding rate coefficient, $k_2$ exhibits an order of dependence slightly higher (equal to 0.7591) than $k_1$ (equal to 0.6082) on the anti-rabbit IgG concentration in solution.

Fig.3a shows the increase in the ratio of the fractal dimensions, $D_{f2}/D_{f1}$ with an increase in the anti-rabbit IgG concentration in solution. In the 50-250 ng/mL anti-rabbit IgG concentration range in solution, the ratio of the fractal dimensions, $D_{f2}/D_{f1}$ is given by:

$$D_{f2}/D_{f1} = (0.8777 \pm 0.0501)[\text{anti-rabbit IgG}]^{0.1319 \pm 0.0486} \quad (3a)$$

Only three data points are available. The fit is reasonable. The availability of more data points would lead to a better fit. The equation provides one with an idea of the change in the degree of heterogeneity on the sensing surface as one goes from the first- to the second-phase of binding. The order of dependence exhibited by the ratio of the fractal dimensions, $D_{f2}/D_{f1}$ on the anti-rabbit IgG concentration in solution is rather small (equal to 0.1319). But, once again, one needs to be reminded that the fractal dimension is based on a log scale and even small changes in the value of the fractal dimension indicate significant changes in the degree of heterogeneity on the sensing surface.

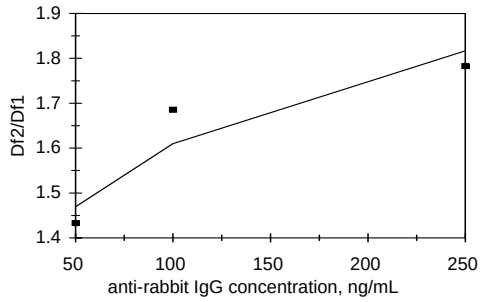


a)

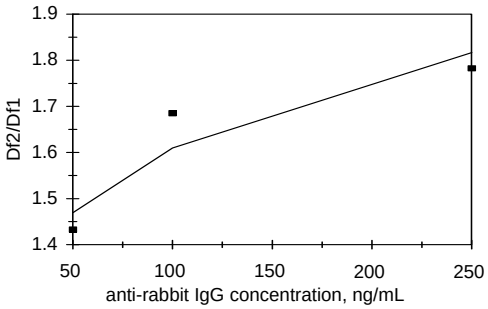


b)

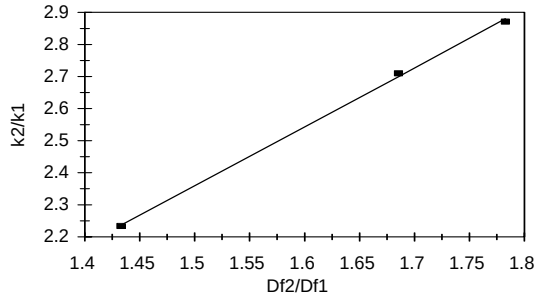


c)

**Fig. 3**.(a) Increase in the fractal dimension ratio, $D_{f2}/D_{f1}$ with an increase in the anti-rabbit IgG concentration (in ng/mL) in solution; (b) Increase in the binding rate coefficient ratio, $k_2/k_1$ with an increase in the anti-rabbit IgG concentration (in ng/mL) in solution; (c) Increase in the binding rate coefficient ratio, $k_2/k_1$ with an increase in the ratio of fractal dimensions, $D_{f2}/D_{f1}$..

Fig.3b shows the increase in the ratio of the binding rate coefficients, $k_2/k_1$ with an increase in the anti-rabbit IgG concentration in solution. In the 50-250 ng/mL anti-rabbit IgG concentration in solution, the ratio of the binding rate coefficients, $k_2/k_1$ is given by:

$$k_2/k_1 = (1.2788 \pm 0.0918)\,[\text{anti-rabbit IgG}]^{0.1509 \pm 0.0607} \quad (3b)$$

Once again, only three data points were available. The availability of more data points would lead to a more reliable fit. The equation does provide one with an estimate of the change in the value of the binding rate coefficients as one goes from the first- to the second-phase of binding as the anti-rabbit IgG concentration in solution changes in the 50-250 ng/mL concentration range. The ratio of the binding rate coefficients, $k_2/k_1$ exhibits a very small order (equal to 0.1509) of dependence on the anti-rabbit IgG concentration in solution.

Fig.3c shows the increase in the ratio of the binding rate coefficients, $k_2/k_1$with an increase in the ratio of fractal dimensions, $D_{f2}/D_{f1}$. In the 50-250 ng/mL anti- rabbit IgG concentration in solution and for the data presented in Fig.3c the ratio of the binding rate coefficients, $k_2/k_1$ is given by:

$$k_2/k_1 = (1.2788 \pm 0.0918)\,[\text{anti-rabbit IgG}]^{0.1509 \pm 0.0607} \quad (3c)$$

The fit is very good. Once again, only three data points were available. The availability of more data points would lead to a more reliable fit. The ratio of the binding rate coefficients, $k_2/k_1$ exhibits an

order of dependence slightly greater than first (equal to 1.1517) order on the ratio of fractal dimensions.

Fig.4a shows the binding of 5 μg/mL monoclonal anti-rabbit antibody in solution to rabbit IgG patterned cells [8]. A single-fractal analysis is adequate to describe the binding kinetics. The values of the binding rate coefficient, k and the fractal dimension, $D_f$ are given in Table 1b.

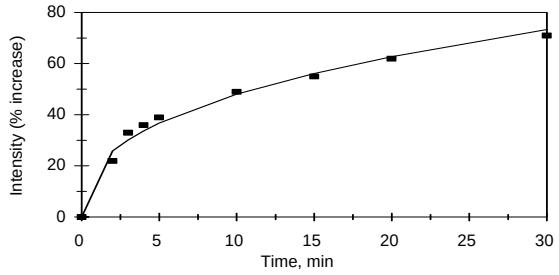


a)

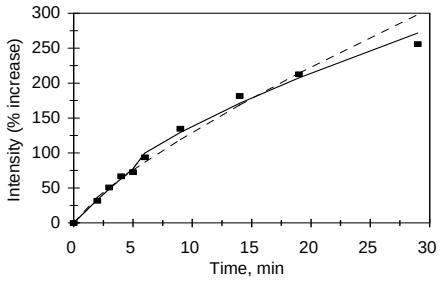


b)

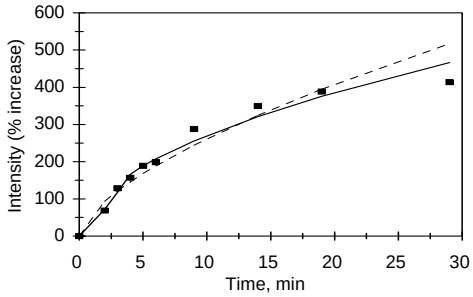


c)

**Fig. 4.** (a) Binding of 5 μg/mL monoclonal anti-rabbit antibody in solution to rabbit IgG patterned cells [2]; (b) Binding of 1 μg/mL anti-mouse gold conjugate antibody in solution to rabbit IgG patterned cells [2]; (c) Binding of 1 μg/mL anti-mouse gold conjugate antibody in solution to rabbit IgG patterned cells [2]; When only a solid line is used then a single-fractal analysis applies. When both a dashed (----) and a solid (____) line are used, then the dashed line is for a single-fractal analysis and the solid line is for a dual-fractal analysis. In this case the solid line provides a better fit.

Fig.4b shows the binding of 1 μg/mL mouse monoclonal anti-rabbit IgG to rabbit IgG patterned cells. This was followed by anti-mouse gold conjugate that Goh et al. [8] used as a secondary label to enhance their diffraction-based sensing for diagnostic purposes. A dual-fractal analysis is required to adequately describe the binding kinetics. The values of (a) the binding rate coefficient, k and the fractal dimension, $D_f$ for a single-fractal analysis and (b) the binding rate coefficients, $k_1$ and $k_2$, and the fractal dimensions, $D_{f1}$ and $D_{f2}$ for a dual-fractal analysis are given in Table 1c.

On using the secondary label (anti-mouse gold conjugate) there is a change in the binding mechanism compared to when it not used. This is because a dual-fractal analysis is required to adequately describe the binding kinetics when the secondary label is used and a single-fractal analysis is adequate to describe the binding kinetics when the secondary label is not used. It is not entirely unexpected that the use of the secondary label leads to a more complex binding mechanism.

Fig.4c shows the binding of 5 μg/mL mouse monoclonal anti-rabbit IgG to rabbit IgG patterned cells. This was followed by anti-mouse gold conjugate that Goh et al. [8] used as a secondary label to enhance their diffraction-based sensing for diagnostic purposes. A dual-fractal analysis is required to adequately describe the binding kinetics. The values of (a) the binding rate coefficient, k and the fractal dimension, $D_f$ for a single-fractal analysis, and (b) the binding rate coefficients, $k_1$ and $k_2$, and the fractal dimensions, $D_{f1}$ and $D_{f2}$ for a dual-fractal analysis are given in Table 1c. It is of interest to note that as one increases the mouse monoclonal anti-rabbit IgG concentration in solution (when the secondary label anti-mouse gold conjugate is present) from 1 to 5 μg/mL, both of the binding rate coefficients, $k_1$ and $k_2$ exhibit increases.

Zybin et al. [3] have used the double-wavelength technique for the on-line monitoring of analyte binding to sensor surfaces using the SPR (surface plasmon resonance) biosensor. These authors have used their recently developed system to analyze and detect short nucleotides of the sequences used for genotyping human hepatitis C viruses. They were able to obtain a selective response to complementary oligonucleotides.

Zybin et al. [3] provide an excellent history of the initial development of the SPR biosensor strating with Leidberg et al. [21] and followed by subsequent modifications of the technique. They emphasize that the improvement in the detection sensitivity has been one of the main goals in improving the SPR sensing technique. For example, immobilization procedures have been optimized [22, 23, 24]. Also, the plasmon layer has been optimized by using bimetallic Ag/Au layers [25, 26]. Zybin et al. [3] indicate that the SPR technique is a highly sensitive technique that may be affected by changes in the surface roughness that influence possible shape changes in the resonance. These authors emphasize that their double-wavelength measurement technique does help alleviate these problems. In essence, in this technique the surface is irradiated by a parallel beam that is composed of two laser beams with different wavelengths.

In their hybridization (binding) experiments Zybin et al. [3] used sequences of the DNA oligonucleotides that were used earlier for their diagnostics of human hepatitis C virus (G) and two types of virus $T_1$ and $T_2$ were also used. The following receptor sequences were used : 5'-CCAAGAAAGGACCCG-3' (G), 5'-CTCCAGGCATTGAGC-3' (T1), and 5'-CAACCCAACGCTACT-3' (T2). Zybin et al. [3] indicate that the analytes in solution were synthetic oligonucleotides of complementary sequence without the thymin spacer. They are designated cG, cT1, and cT2, respectively.

Fig.5a shows the binding (hybridization) of G-HCV-c of the sequence 5'-TTTCGGGTCCTTTCTTGG3' to the spot coated with the complementary oligonucleotide G-HCV of the sequence 5'-TTTTTCCAAGAAAGGACC-3'. A dual-fractal analysis is required to adequately describe the hybridization (binding) kinetics. The values of (a) the binding rate coefficient, k and the fractal dimension, $D_f$ for a single-fractal analysis, and (b) the binding rate coefficients, $k_1$ and $k_2$ and the fractal dimensions, $D_{f1}$ and $D_{f2}$ for a dual-fractal analysis are given in Table 2.

Fig.5b shows the selective hybridization (binding) of G-HCV-c in a mixture of G-HCV-c and $T_2$-HCV-c in solution to G-HCV and $T_2$-HCV complementary sequences immobilized at different spots. A dual-fractal analysis is required to adequately describe the hybridization (binding) kinetics. The values of (a) the hybridization (binding) rate coefficient, k, and the fractal dimension, $D_f$ for a single-fractal analysis and (b) the hybridization (binding) rate coefficients, $k_1$ and $k_2$ and the fractal dimensions, $D_{f1}$ and $D_{f2}$ for a dual-fractal analysis are given in Table 2.

Fig.5c shows the selective hybridization (binding) of $T_2$-HCV-c in a mixture of G-HCV-c and $T_2$-HCV-c in solution to G-HCV and $T_2$-HCV complementary sequences immobilized at different spots. A dual-fractal analysis is, once again, required to adequately describe the hybridization (binding) kinetics. The values of (a) the hybridization (binding) rate coefficient, k, and the fractal dimension, $D_f$ for a single-fractal analysis, and (b) the hybridization (binding) rate coefficients, $k_1$ and $k_2$ and the fractal dimensions, $D_{f1}$ and $D_{f2}$ for a dual-fractal analysis are given in Table 2.

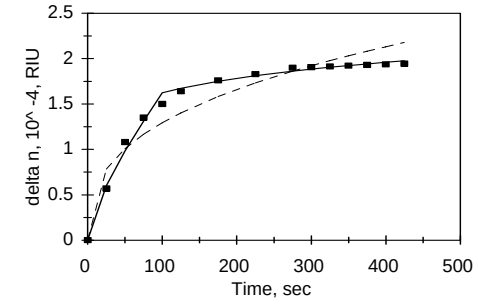


a)

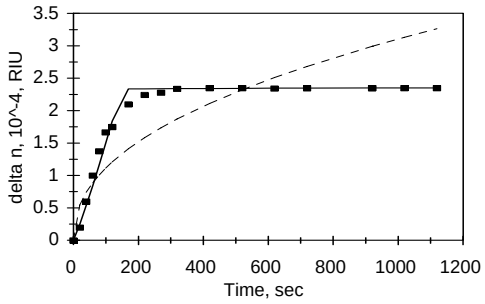


b)

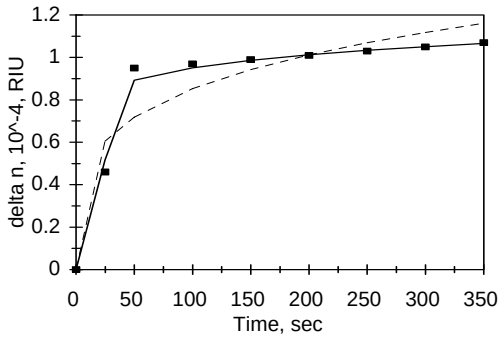


c)

**Fig. 5**. (a) Binding and hybridization of G-HCV-c of the sequence 5'-TTT CGG GTC CTT TCT TGG3' to the spot coated with the complementary oligonuclotide of the sequence 5'-TTT TTC CAA GAA AGG ACC-3' [3]; (b) Selective hybridization and binding of G-HCV-c in solution to G-HCV immobilized on a spot surface [3]; (c) Selective hybridization and binding of $T_2$-HCV-c in solution to $T_2$-HCV immobilized on a spot surface [3]. When only a solid line is used then a single-fractal analysis applies. When both a dashed (----) and a solid (____) line are used, then the dashed line is for a single-fractal analysis and the solid line is for a dual-fractal analysis. In this case the solid line provides a better fit.

**Table 2.** Binding rate coefficients and fractal dimensions for the hybridization of (a) G-HCV-c of the sequence 5'-TTT CGG GTC CTT TCT TGG3' to the spot coated with complementary oligonucleotide G-HCV of the sequence 5'-TTT TTC CAA GAA AGG ACC-3', (b) G-HCV-c to the spot coated with G-HCV, and $T_2$–HCV-c to the spot coated with $T_2$ –HCV, and (c) (G-HCV-c) + ($T_1$ –HCV-c) + ($T_2$ –HCV-c) to the spot coated with G-HCV, $T_1$ –HCV, and $T_2$ –HCV [3].

| Analyte in solution/Receptor on spot surface | **k** | **$k_1$** | **$k_2$** | **$D_f$** | **$D_{f1}$** | **$D_{f2}$** |
|---|---|---|---|---|---|---|
| (a) G-HCV-c/G-HCV | 0.2463 ±0.0359 | 0.0611 ±0.0060 | 0.8676 ±0.0121 | 2.2796 ±0.0860 | 1.5796 ±0.1788 | 2.7282 ±0.02338 |
| (b) Selective hybridization of G-HCV-c and $T_2$ –HCV-c/ G-HCV and $T_2$ –HCV (complementary sequences immobilized at different spots) | 0.1451 ±0.0652 | 0.00886 ±0.00192 | 2.2926 ±0.0009 | 2.1126 ±0.1483 | 0.7706 ±0.2214 | 2.9928 ±0.001598 |
| G-HCV-c/G-HCV | 0.2734 ±0.0524 | 0.09150 ±0.0305 | 0.6247 ±0.0025 | 2.5062 ±0.1431 | 1.9236 ±0.5866 | 2.8176 ±0.01196 |
| $T_2$ –HCV –c/$T_2$ –HCV | | | | | | |
| (c) (G-HCV-c) + ($T_1$ – HCV–c) + ($T_2$ –HCV–c)/G-HCV | 0.05855 ±0.01554 | 0.005446 ±0.000724 | 0.6989 ±0.0130 | 1.7330 ±0.1424 | 0.5770 ±0.1963 | 2.6158 ±0.0304 |
| (G-HCV-c) + ($T_1$ –HCV–c) + ($T_2$ –HCV –c)/ $T_1$-HCV | 0.2297 ±0.0258 | 0.06072 ±0.00582 | 0.3233 ±0.0107 | 2.5530 ±0.06450 | 1.8792 ±0.1756 | 2.6810 ±0.06454 |
| (G-HCV-c) + ($T_1$ –HCV–c) + ($T_2$ –HCV–c)/ $T_2$-HCV | 0.01484 ±0.00312 | 0.002039 ±0.000074 | 0.1249 ±0.0050 | 1.4862 ±0.1157 | 0.5186 ±0.06816 | 2.2442 ±0.05452 |

Note that the selective hybridization rate coefficients, $k_1$ for G-HCV-c/G-HCV is lower than that for $T_2$-HCV-c/$T_2$-HCV. However, the selective hybridization rate coefficient, $k_2$ for G-HCV-c/G-HCV is higher than that for $T_2$-HCV-c/$T_2$-HCV. It is of interest to note that the corresponding fractal dimensions also follow similar trends. In this case, higher fractal dimensions or higher degrees of heterogeneity on the spot surface lead to higher hybridization (binding) rate coefficients and vice versa. For example, the fractal dimension, $D_{f1}$ values for G-HCV-c/G-HCV and $T_2$-HCV-c/$T_2$-HCV are 0.7706 and 1.9236, respectively. Correspondingly, the hybridization (binding) rate coefficients, $k_1$ are 0.0086 and 0.09150, respectively. Similarly, the fractal dimension, $D_{f2}$ values for G-HCV-c/G-HCV and $T_2$-HCV-c/$T_2$-HCV are 2.9928 and 2.8176, respectively. Correspondingly, the hybridization (binding) rate coefficients, $k_2$ are 2.2926 and 0.6247, respectively.

Fig.6a shows the hybridization (binding) of (G-HCV-c) + ($T_1$–HCV-c) + ($T_2$–HCV-c) in solution to G-HCV immobilized on a spot surface [3]. A dual-fractal analysis is required to adequately describe the hybridization (binding) kinetics. The values of (a) the binding rate coefficient, k and the fractal dimension, $D_f$, and (b) the binding rate coefficients, $k_1$ and $k_2$ and the fractal dimensions, $D_{f1}$ and $D_{f2}$ for a dual-fractal analysis are given in Table 2.

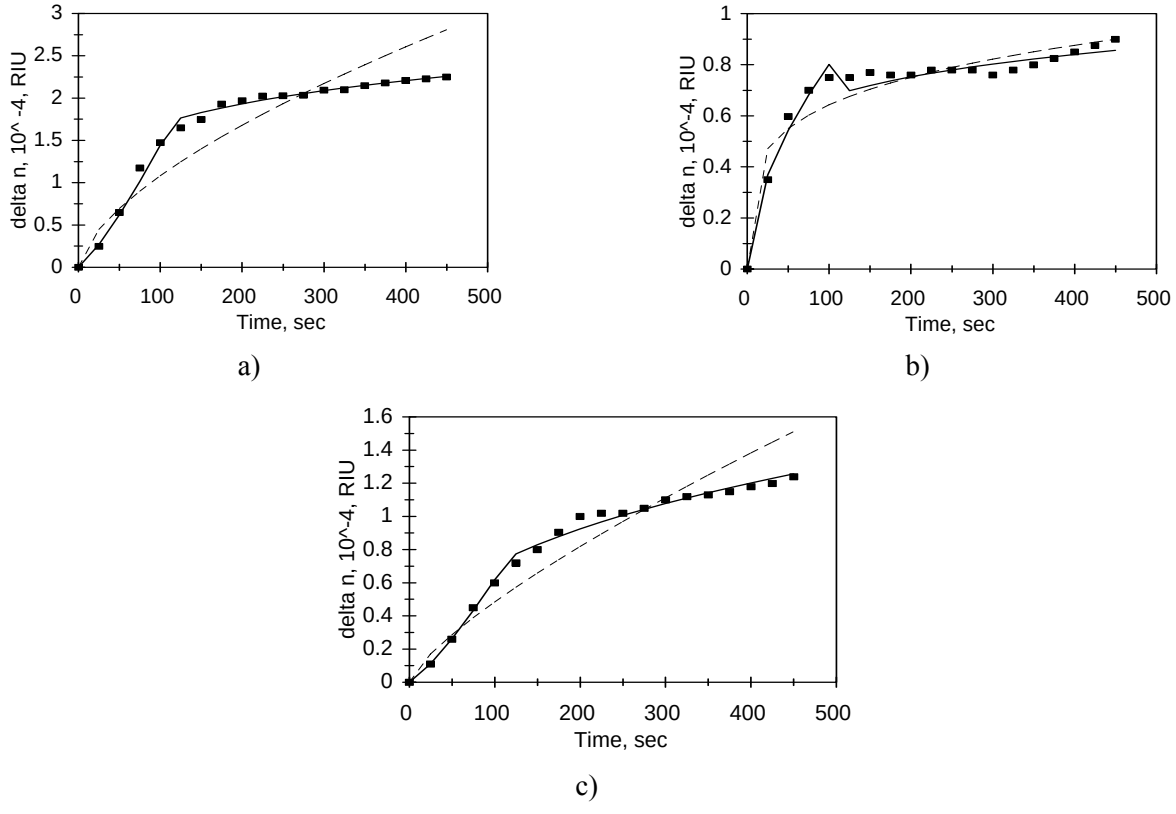


**Fig. 6**. (a) Binding and hybridization of (G-HCV-c) + ($T_1$ –HCV-c) + ($T_2$ –HCV-c) in solution to G-HCV immobilized on a spot surface[3]; (b) Binding and hybridization of (G-HCV-c) + ($T_1$ –HCV-c) +($T_2$ –HCV-c) in solution to $T_1$-HCV immobilized on a spot surface [3]; (c) Binding and hybridization of (G-HCV-c) + ($T_1$ – HCV-c) + ($T_2$ –HCV-c) in solution to $T_2$-HCV immobilized on a spot surface [3]. When only a solid line is used then a single-fractal analysis applies. When both a dashed (----) and a solid (____) line are used, then the dashed line is for a single-fractal analysis and the solid line is for a dual-fractal analysis. In this case the solid line provides a better fit.

Fig.6b shows the hybridization (binding) of (G-HCV-c) + ($T_1$–HCV-c) + ($T_2$–HCV-c) in solution to $T_1$-HCV immobilized on a spot surface [3]. Once again, a dual-fractal analysis is required to adequately describe the hybridization (binding) kinetics. The values of (a) the binding rate coefficient,

k and the fractal dimension, $D_f$ , and (b) the binding rate coefficients, $k_1$ and $k_2$ and the fractal dimensions, $D_{f1}$ and $D_{f2}$ for a dual-fractal analysis are given in Table 2.
Fig.6c shows the hybridization (binding) of (G-HCV-c) + ($T_1$–HCV-c) + ($T_2$–HCV-c) in solution to $T_2$-HCV immobilized on a spot surface [3]. Once again, a dual-fractal analysis is required to adequately describe the hybridization (binding) kinetics. The values of (a) the binding rate coefficient, k and the fractal dimension, $D_f$ and (b) the binding rate coefficients, $k_1$ and $k_2$ and the fractal dimensions, $D_{f1}$ and $D_{f2}$ for a dual-fractal analysis are given in Table 2.

It is of interest to note that the fractal dimension, $D_{f1}$ increases in the sequence $T_2$–HCV-c, G-HCV-c and $T_1$–HCV-c immobilized on the spot surface and the corresponding binding rate coefficients, $k_1$ also increase in the same sequence $T_2$–HCV-c, G-HCV-c and $T_1$–HCV-c.

Tables 2 and 2b and Fig.7a show the increase in the (hybridization) binding rate coefficient, $k_1$ with an increase in the fractal dimension, $D_{f1}$. For the binding of G-HCV–c in solution to G-HCV immobilized on the spot surface and for the selective hybridization of G-HCV-c and $T_2$-HCV-c in solution to complementary sequences immobilized at different spot surfaces, the binding rate coefficient, $k_1$ is given by:

$$k_1 = (0.01762 \pm 0.00141)\, D_{f1}^{2.5894 \pm 0.1128} \tag{4a}$$

Only three data points are available. The fit is good. The availability of more data points would lead to a more reliable fit. The binding rate coefficient, $k_1$ is sensitive to the degree of heterogeneity that exists on the spot surface, as noted by the slightly greater than two and one half (equal to 2.5894) order of dependence exhibited.

Fig.7b shows the increase in the (hybridization) ratio of the binding rate coefficients, $k_2/k_1$ with an increase in the ratio of the fractal dimensions, $D_{f2}/D_{f1}$. For the binding of G-HCV–c in solution to G-HCV immobilized on the spot surface and for the selective hybridization of G-HCV-c and $T_2$-HCV-c in solution to complementary sequences immobilized at different spot surfaces, the ratio of the binding rate coefficients, $k_2/k_1$ is given by:

$$k_2/k_1 = (1.7717 \pm 0.1682)\, (D_{f2}/D_{f1})^{3.6824 \pm 0.1229} \tag{4b}$$

Only three data points are available. The fit is good. The availability of more data points would lead to a more reliable fit. The ratio of the binding rate coefficients, $k_2/k_1$ is very sensitive to the degree of heterogeneity that exists on the spot surface, as noted by the order between three and one half and fourth (equal to 3.6824) exhibited.

Table 2 and Fig.7c shows the increase in the (hybridization) binding rate coefficient, $k_1$ with an increase in the fractal dimension, $D_{f1}$. In this case, the binding rate coefficient, $k_1$ is given by:

$$k_1 = (0.01387 \pm 0.00936)\, D_{f1}^{2.3901 \pm 0.5104} \tag{4c}$$

Only three data points are available. The fit is good. The availability of more data points would lead to a more reliable fit. The binding rate coefficient, $k_1$ is sensitive to the degree of heterogeneity that exists on the spot surface, as noted by the 2.3901 order of dependence exhibited.

Fig. 7d shows the increase in the (hybridization) ratio of the binding rate coefficients, $k_2/k_1$ with an increase in the ratio of the fractal dimensions, $D_{f2}/D_{f1}$. For the data presented in Table 2 the ratio of the binding rate coefficients, $k_2/k_1$ is given by:

$$k_2/k_1 = (2.1627 \pm 1.1995)\, (D_{f2}/D_{f1})^{2.4996 \pm 0.4767} \tag{4d}$$

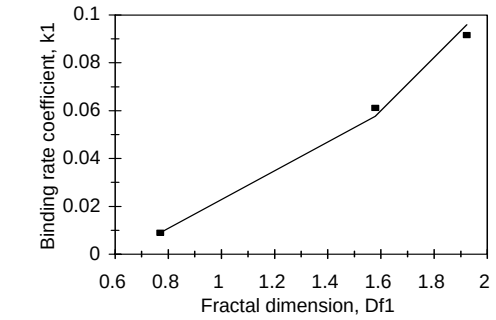


a)

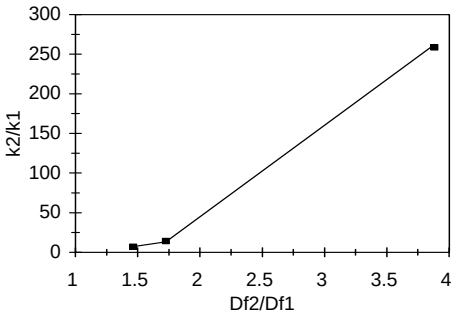


b)

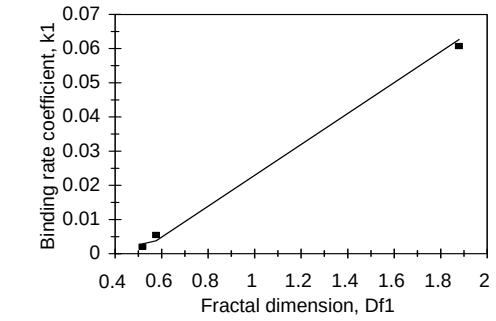


c)

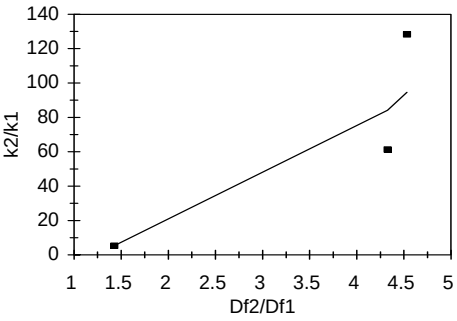


d)

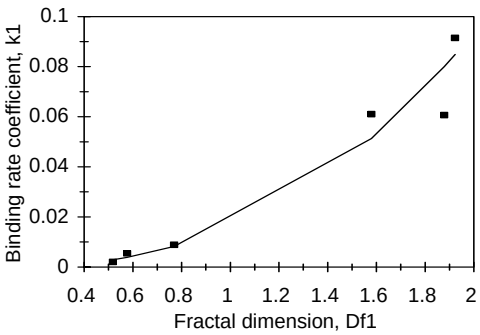


e)

**Fig. 7.** (a) Increase in the binding rate coefficient, $k_1$ with an increase in the fractal dimension, $D_{f1}$; (b) Increase in the ratio of binding rate coefficients, $k_2/k_1$ with an increase in the fractal dimension ratio, $D_{f2}/D_{f1}$; (c) Increase in the binding rate coefficient, $k_1$ with an increase in the fractal dimension, $D_{f1}$; (d) Increase in the ratio of binding rate coefficients, $k_2/k_1$ with an increase in the fractal dimension ratio, $D_{f2}/D_{f1}$; (e) Increase in the binding rate coefficient, $k_1$ with an increase in the fractal dimension, $D_{f1}$.

Only three data points are available. The fit is good. The availability of more data points would lead to a more reliable fit. The ratio of the binding rate coefficients, $k_2/k_1$ is sensitive to the ratio of the fractal dimensions, $D_{f2}/D_{f1}$ that exists on the spot surface, as noted by the very close to two and one-half order of dependence (equal to 2.4996) exhibited.

Tables 2 and Fig.7e show the increase in the (hybridization) binding rate coefficient, $k_1$ with an increase in the fractal dimension, $D_{f1}$. In this figure we have plotted the results presented in Figure 7a and 7c on one plot. This was to see if it made a lot of difference on plotting both of these types of analyte-receptor systems on one plot. In this case, the binding rate coefficient, $k_1$ is given by:

$$k_1 = (0.01596 \pm 0.00568)\, D_{f1}^{2.5564 \pm 0.2256} \tag{4e}$$

In this case since two sets of data are plotted together, six data points are available. Considering that data from two different sets are plotted together, the fit is good. The availability of more data points would nevertheless lead to a more reliable fit. The binding rate coefficient, $k_1$ is sensitive to the degree of heterogeneity that exists on the spot surface, as noted by the 2.5564 order of dependence exhibited.

Gerdon et al. [4] recently indicate that there is a need to develop a label-free, fast-responsive, quantitative assay for the detection of 3D substrates and multilayer adsorptions [27]. They indicate that

two techniques that use wave propagation techniques have gained prominence. They are the surface plasmon resonance (SPR) and the Quartz Crystal Microbalance (QCM) techniques. Gerdon et al. [4] indicate that the QCM technique uses acoustic waves, whereas the SPR technique uses optical waves. The QCM technique measures the acoustic impedance minimum, and the SPR technique measures the angle of reflection minimum. These authors emphasize the ability of the QCM technique to work with 3D substrates and multilayer adsorptions.

Fig.8 shows the binding of 4.1 μM Tiop (Tiopronin)-MPC (Monolayer protected clusters) in solution to polyclonal anti-glutathione + protein A immobilized on a quartz crystal microbalance [4]. The plot of the binding is a straight line. A single-fractal analysis is adequate to describe the binding kinetics. The binding rate coefficient, k value is 0.006, and the fractal dimension, $D_f$ value is 2.0. This $D_f$ equal to 2.0 value is the value of a homogeneous distribution in two-dimensional space.

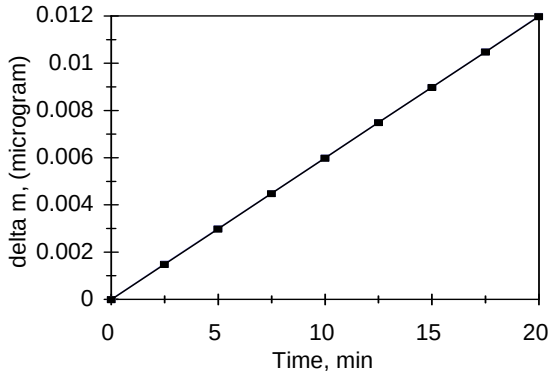


**Fig.8**. Binding of 4.1 μM Tiop (Tiopronin)-MPC (monolayer protected clusters) in solution to polyclonal anti-glutathione + protein A immobilized on a quartz crystal microbalance (QCM) [4].

Fig.9a shows the binding and dissociation kinetics of 2.3 μM glutathione (GSH)-monolayer protected clusters (MPC) in solution to polyclonal antibody (polyclonal anti-GSH) + protein A immobilized on a quartz crystal microbalance (QCM) [4]. A dual-fractal analysis is required to adequately describe the binding kinetics. A single-fractal analysis is adequate to describe the dissociation kinetics. The values of (a) the binding rate coefficient, k and the fractal dimension, $D_f$ for a single-fractal analysis, and (b) the binding rate coefficients, $k_1$ and $k_2$, and the fractal dimensions, $D_{f1}$ and $D_{f2}$ for a dual-fractal analysis are given in Table 3.

Fig.9b shows the binding and dissociation kinetics of 4.5 μM glutathione (GSH)-monolayer protected clusters (MPC) in solution to polyclonal antibody (polyclonal anti-GSH) + protein A immobilized on a quartz crystal microbalance (QCM) [4]. A dual-fractal analysis is required to adequately describe the binding kinetics. A single-fractal analysis is adequate to describe the dissociation kinetics. The values of (a) the binding rate coefficient, k and the fractal dimension, $D_f$ for a single-fractal analysis, and (b) the binding rate coefficients, $k_1$ and $k_2$, and the fractal dimensions, $D_{f1}$ and $D_{f2}$ for a dual-fractal analysis are given in Table 1c. It is of interest to note that as the glutathione (GSH)-MPC concentration in solution increases by almost a factor two from 2.3 to 4.5 μM, the binding rate coefficient, $k_1$ value increases by a factor of 1.752 from a value of 0.001145 to 0.002007 and the binding rate coefficient, $k_2$ value increases by a factor of 1.902 from a value of 0.0256 to 0.04868.

Fig.9c shows the binding and dissociation kinetics of 9.1 μM glutathione (GSH)-monolayer protected clusters (MPC) in solution to polyclonal antibody (polyclonal anti-GSH) + protein A immobilized on a quartz crystal microbalance (QCM) [4]. A dual-fractal analysis is required to adequately describe the binding kinetics. A single-fractal analysis is adequate to describe the dissociation kinetics. The values of (a) the binding rate coefficient, k and the fractal dimension, $D_f$ for a single-fractal analysis, and (b)

the binding rate coefficients, $k_1$ and $k_2$, and the fractal dimensions, $D_{f1}$ and $D_{f2}$ for a dual-fractal analysis are given in Table 1c. It is of interest to note that as the glutathione (GSH)-MPC concentration in solution increases by almost a factor two from 4.5 to 9.1 μM, the binding rate coefficient, $k_1$ value increases by a factor of 10.36 from a value of 0.002007 to 0.02079 and the binding rate coefficient, $k_2$ value increases by a factor of 1.064 from a value of 0.04868 to 0.05178.

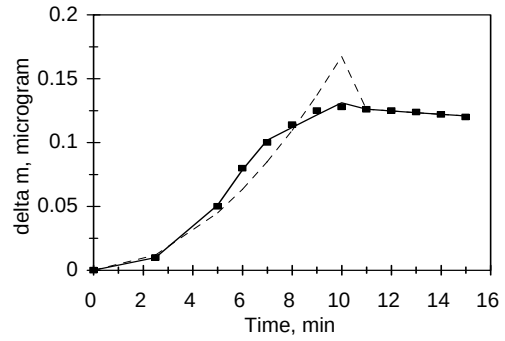


a)

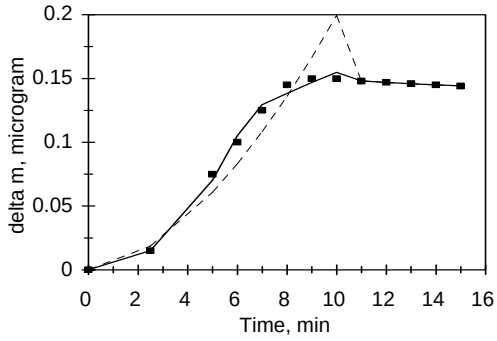


b)

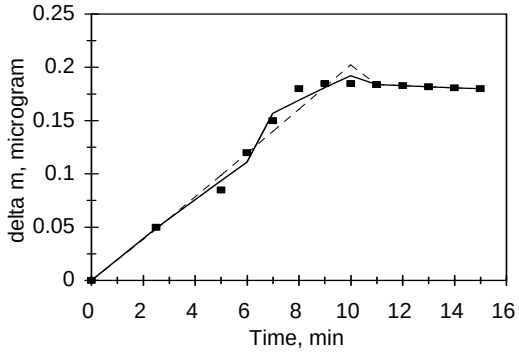


c)

**Fig. 9**. Binding and dissociation of different concentrations (in μM) of GSH (Glutathione)-MPC (monolayer protected clusters) in solution to polyclonal antibody (polyclonal anti-GSH) + protein A immobilized on a quartz crystal microbalance (QCM) [4]): (a) 2.3; (b) 4.5; (c) 9.1. When only a solid line is used then a single-fractal analysis applies. When both a dashed (----) and a solid (___) line are used, the dashed line is for a single-fractal analysis and the solid line is for a dual-fractal analysis. In this case the solid line provides a better fit.

**Table. 3.** Binding and dissociation rate coefficients for different concentrations (in μM) for GSH (Glutathione)-MPC (monolayer protected clusters) in solution to polyclonal antibody (polyclonal anti-GSH) + protein A immobilized on a quartz crystal microbalance (QCM) [4].

| GSH-MPC, μM | **k** | **$k_1$** | **$k_2$** | **$k_d$** |
|---|---|---|---|---|
| 2.3 | 0.002097<br>±0.00045 | 0.001145<br>±0.00003 | 0.0256<br>±0.00081 | 0.001823<br>±0.000254 |
| 4.5 | 0.003858<br>±0.000945 | 0.002007<br>±0.000174 | 0.04868<br>±0.00246 | 0.001943<br>±0.000071 |
| 9.1 | 0.01867<br>±0.00280 | 0.02079<br>±0.00280 | 0.05178<br>±0.00331 | 0.001<br>± 0 |

**Table. 3b.** Fractal dimensions for the binding and the dissociation phase for different concentrations (in μM) for GSH (Glutathione-MPC (monolayer protected clusters) in solution to polyclonal antibody (polyclonal anti-GSH) + protein A immobilized on a quartz crystal microbalance (QCM) [4].

| GSH-MPC, μM | **$D_f$** | **$D_{f1}$** | **$D_{f2}$** | **$D_{fd}$** |
|---|---|---|---|---|
| 2.3 | 0.0<br>+0.3550 | 0.0<br>+0.08752 | 1.5806<br>±0.2356 | 2.9964<br>±0.1027 |
| 4.5 | 0.0<br>+0.3814 | 0.0<br>+0.2544 | 1.9948<br>±0.3696 | 1.6384<br>±0.05694 |
| 9.1 | 0.9294<br>±0.1744 | 1.1298<br>±0.3850 | 1.8608<br>±0.4672 | 1.0<br>± 1.4E-16 |

Fig.10a and Table 3a show the increase in the binding rate coefficient, $k_1$ with an increase in the GSH-MPC concentration in solution. In the 2.3 to 9.1 μM GSH-MPC concentration range, the binding rate coefficient, $k_1$ is given by:

$$k_1 = (0.000147 \pm 0.000147)\,[\text{GSH-MPC}]^{2.1178 \pm 0.7164} \tag{5a}$$

The fit is quite good. Only three data points are available. The availability of more data points would lead to a more reliable fit. The binding rate coefficient, $k_1$ is sensitive to the [GSH-MPC] concentration in solution as noted by the slightly higher than second order (equal to 2.1177) order of dependence exhibited.

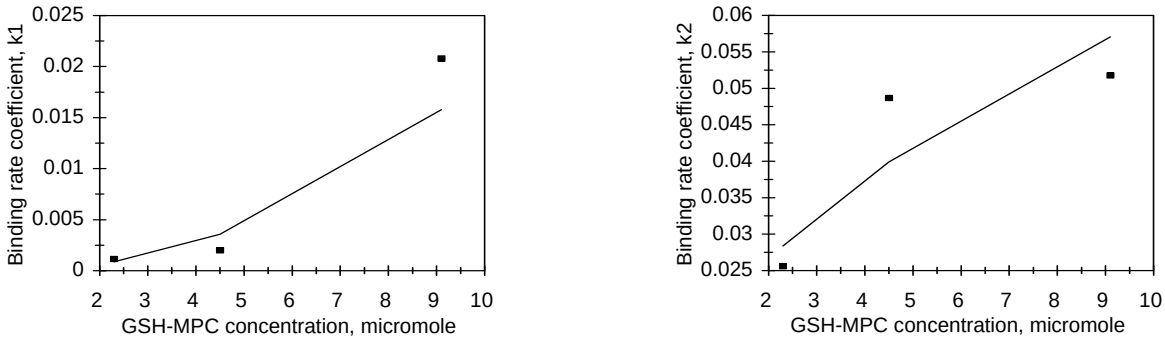


**Fig. 10**. (a) Increase in the binding rate coefficient, $k_1$ with an increase in the GSH-MPC concentration (in μM) in solution; (b) Increase in the binding rate coefficient, $k_2$ with an increase in the GSH-MPC concentration (in μM) in solution.

Fig.10b and Table 3a show the increase in the binding rate coefficient, $k_2$ with an increase in the GSH-MPC concentration in solution. In the 2.3 to 9.1 μM GSH-MPC concentration range, the binding rate coefficient, $k_2$ is given by:

$$k_2 = (0.01857 \pm 0.00513)\,[\text{GSH-MPC}]^{0.5084 \pm 0.2507} \tag{5b}$$

The fit is quite good. Only three data points are available. The availability of more data points would lead to a more reliable fit. The binding rate coefficient, $k_2$ is only mildly sensitive to the [GSH-MPC] concentration in solution as noted by the close to one-half order (equal to 0.5084) order of dependence exhibited.

Table 3a and Fig.11a show the increase in the binding rate coefficient, $k_1$ with an increase in the fractal dimension, $D_{f1}$. In the 2.3-9.1 μM GSH-MPC concentration range, the binding rate coefficient, $k_1$ is given by:

$$k_1 = (0.01509 \pm 0.0104) D_{f1}^{1.1611 \pm 0.2899} \tag{6a}$$

The fit is good. Only three data points are available. The availability of more data points would lead to a more reliable fit. The binding rate coefficient, $k_1$ exhibits slightly more than first-order (equal to 1.1611) order of dependence on the fractal dimension $D_{f1,}$ or the degree of heterogeneity that exists on the quartz crystal microbalance surface.

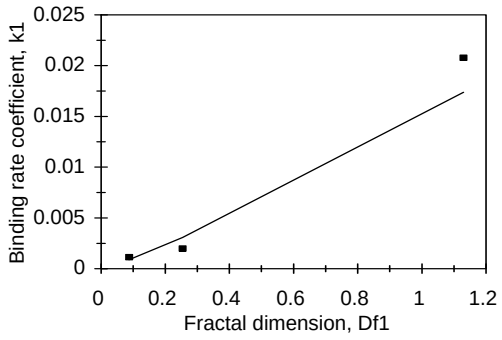


a)

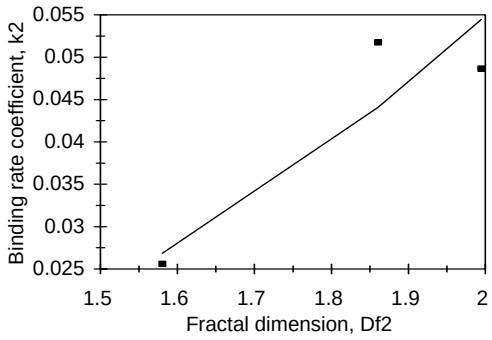


b)

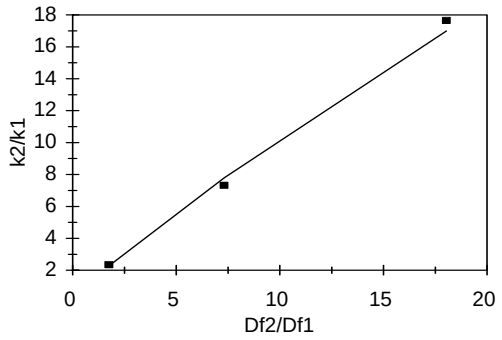


c)

**Fig. 11.** (a) Increase in the binding rate coefficient, $k_1$ with an increase in the fractal dimension, $D_{f1}$; (b) Increase in the binding rate coefficient, $k_2$ with an increase in the fractal dimension, $D_{f2}$; (c) Increase in the ratio of binding rate coefficients, $k_2/k_1$ with an increase in the fractal dimension ratio, $D_{f2}/D_{f1}$.

Table 3a and Fig.11b show the increase in the binding rate coefficient, $k_2$ with an increase in the fractal dimension, $D_{f2}$. In the 2.3-9.1 μM GSH-MPC concentration range, the binding rate coefficient, $k_2$ is given by:

$$k_2 = (0.006689 \pm 0.001496)D_{f2}^{3.0371 \pm 1.1939} \quad (6b)$$

The fit is good. Only three data points are available. The availability of more data points would lead to a more reliable fit. The binding rate coefficient, $k_1$ exhibits slightly more than first-order (equal to 1.1611) order of dependence on the fractal dimension $D_{f1,}$ or the degree of heterogeneity that exists on the quartz crystal microbalance surface.

Fig.11c show the increase in the ratio of the binding rate coefficients, $k_2/k_1$ with an increase in the fractal dimension ratio, $D_{f2}/D_{f1}$. In the 2.3-9.1 μM GSH-MPC concentration range, the ratio of the binding rate coefficients, $k_2/k_1$ is given by:

$$k_2/k_1 = (1.3983 \pm 0.1134)(D_{f2}/D_{f1})^{0.8632 \pm 0.04704} \quad (6c)$$

The fit is good. Only three data points are available. The availability of more data points would lead to a more reliable fit. The ratio of the binding rate coefficients, $k_2/k_1$ exhibits less than a first-order (equal to 0.8632) order of dependence on the ratio of fractal dimensions, $(D_{f2}/D_{f1})$ that exists on the QCM surface.

Volland et al. [5] have recently suggested some of the desirable characteristics for immunosensors or biosensors. These include: recognition of different analytes present in solution, preferably simultaneously, response in a few minutes, field analysis(autonomy, and ruggedness), continuous-flow analysis, and (d) regeneration of the sensor, or repeated use. The last characteristic is often difficult to realize in practice, and singe-use biosensors have been developed. Volland et al. [5] have recently developed a new concept of an immunosensor that permits a sensitive measurement as well as non

aggressive regeneration [28]. This new method is termed as solid-phase immobilized tripod for fluorescent renewable immunoassay (SPIT-FRI).

Fig.12a shows the binding of 1 μM substance P (neuropeptide) (SP) in solution to quencher-labeled mAb (monoclonal antibody) SP31 using the SPIT-FRI procedure [5]. A single-fractal analysis is adequate to describe the binding kinetics. A dual-fractal analysis is required to adequately describe the dissociation kinetics. The values of (a) the binding rate coefficient, k and the fractal dimension, $D_f$ for a single-fractal analysis, (b) the dissociation rate coefficient, $k_d$ and the fractal dimension, $D_{fd}$ for a single-fractal analysis and (c) the dissociation rate coefficients, $k_{d1}$ and $k_{d2}$ and the fractal dimensions, $D_{fd1}$ and $D_{fd2}$ for a dual-fractal analysis are given in Tables 4a and 4b.

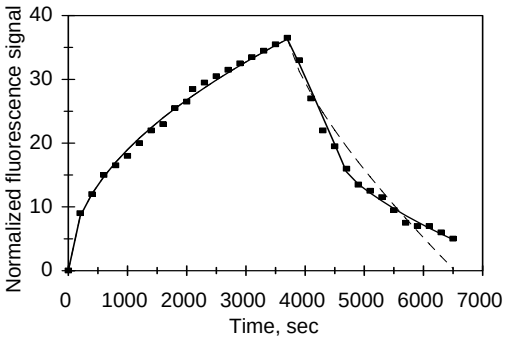


a)

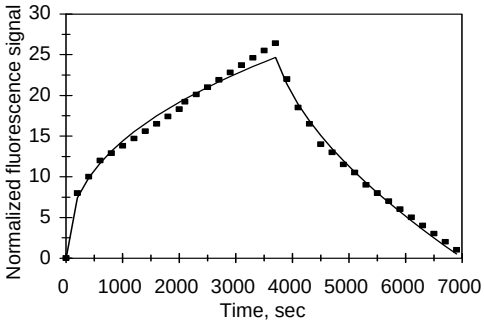


b)

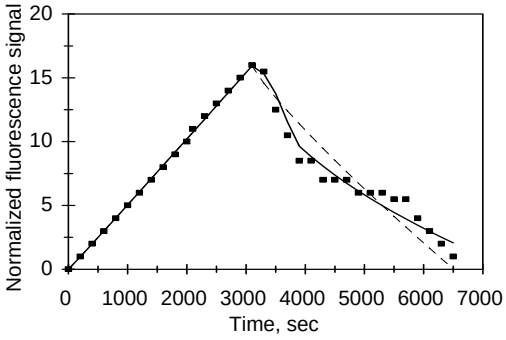


c)

**Fig. 12.** (a) Binding and dissociation of different concentrations (in μM) of substance P (neuropeptide) (SP) in solution to quencher-labeled MAb SP 31 using the SPIT-FRI (solid-phase immobilized tripod for fluorescence immunoassay) procedure [5]): (a) 1; (b) 0.01; (c) 0.1. When only a solid line is used then a single-fractal analysis applies. When both a dashed (----) and a solid (____) line are used, then the dashed line is for a single-fractal analysis and the solid line is for a dual-fractal analysis. In this case the solid line provides a better fit.

Fig.12b shows the binding of 0.1 μM substance P (neuropeptide) (SP) in solution to quencher-labeled mAb (monoclonal antibody) SP31 using the SPIT-FRI procedure [5]. A single-fractal analysis is adequate to describe the binding as well as the dissociation kinetics. The values of (a) the binding rate coefficient, k and the fractal dimension, $D_f$ for a single-fractal analysis and (b) the dissociation rate coefficient, $k_d$ for and the fractal dimension, $D_{fd}$ for a single-fractal analysis are given in Tables 4a and 4b.

Fig.12c shows the binding of 0.01 μM substance P (neuropeptide) (SP) in solution to quencher-labeled mAb (monoclonal antibody) SP31 using the SPIT-FRI procedure [5]. Once again, a single-fractal analysis is adequate to describe the binding kinetics. A dual-fractal analysis is required to adequately describe the dissociation kinetics. The values of (a) the binding rate coefficient, k and the fractal dimension, $D_f$ for a single-fractal analysis, (b) the dissociation rate coefficient, $k_d$ and the fractal dimension, $D_{fd}$ for a single-fractal analysis, and (c) the dissociation rate coefficients, $k_{d1}$ and $k_{d2}$ and the fractal dimensions, $D_{fd1}$ and $D_{fd2}$ for a dual-fractal analysis are given in Tables 4a and 4b.

**Table 4 a.** Binding and dissociation rate coefficients for the interaction of substance P (neuropeptide) (SP) at different concentrations in solution to quencher-labeled mAb SP31 using the SPIT-FRI (solid-phase immobilized tripod for fluorescent renewable immunoassay) procedure [5].

| Analyte in solution, μM | **k** | **$k_1$** | **$k_2$** | **$k_d$** | **$k_{d1}$** | **$k_{d2}$** |
|---|---|---|---|---|---|---|
| 1 | 0.6191 ±0.0176 | na | na | 0.1089 ±0.020 | 0.01781 ±0.00270 | 1.5674 ±0.0347 |
| 0.1 | 0.8364 ±0.0388 | na | na | 0.2123 ±0.0103 | na | na |
| 0.01 | 0.004514 ±0.000070 | na | na | 0.01499 ±0.00586 | 0.000083 ±0.000041 | 0.1697 ±0.0134 |

**Table 4b.** Fractal dimensions for the binding and the dissociation phase for the interaction of substance P (neuropeptide) (SP) at different concentrations in soluiton to quencher-labeled mAb SP31 using the SPIT-FRI (solid-phase immobilized tripod for fluorescent renewable immunoassay) procedure [5].

| Analyte in solution, μM | $D_f$ | $D_{f1}$ | $D_{f2}$ | $D_{fd}$ | $D_{fd1}$ | $D_{fd2}$ |
|---|---|---|---|---|---|---|
| 1 | 2.0088 ±0.0166 | na | na | 1.5372 ±10.1158 | 0.9522 ±0.1908 | 2.2430 ±0.05968 |
| 0.1 | 2.1762 ±0.02684 | na | na | 1.8084 ±0.03096 | na | na |
| 0.01 | 0.9676 ±0.010122 | na | na | 1.2856 ±0.1861 | 0.0 +0.6220 | 1.9158 ±0.1078 |

Tables 4a and 4b and Fig.13a show the increase in the binding rate coefficient, k with an increase in the fractal dimension, $D_f$. In the 0.01 to 1.0 μM substance P (neuropeptide) concentration range in solution the binding rate coefficient, k is given by:

$$k = (0.005668 \pm 0.000978) D_f^{6.5595 \pm 0.2519} \quad (7a)$$

The fit is good. Only three data points are available. The availability of more data points would lead to a more reliable fit. The binding rate coefficient, k is very sensitive to the degree of heterogeneity or the fractal dimension, $D_f$ as noted by the order between six and seven (equal to 6.5595) exhibited.

Affinity values are of interest to practicing biosensorists. Affinity may be defined as the ratio of the binding to the dissociation rate coefficient. There are few points available if one were to look at either the single-fractal analysis or the dual-fractal analysis used to model the dissociation kinetics. In order to offset this drawback we will plot the affinity values that include both the single-fractal analysis as well as the dual-fractal analysis used to model the dissocation kinetics on a single plot. In other words, affinity may be defined as $k/k_d$, $k/k_{d1}$, or $k/k_{d2}$ as far as this plot is concerned.

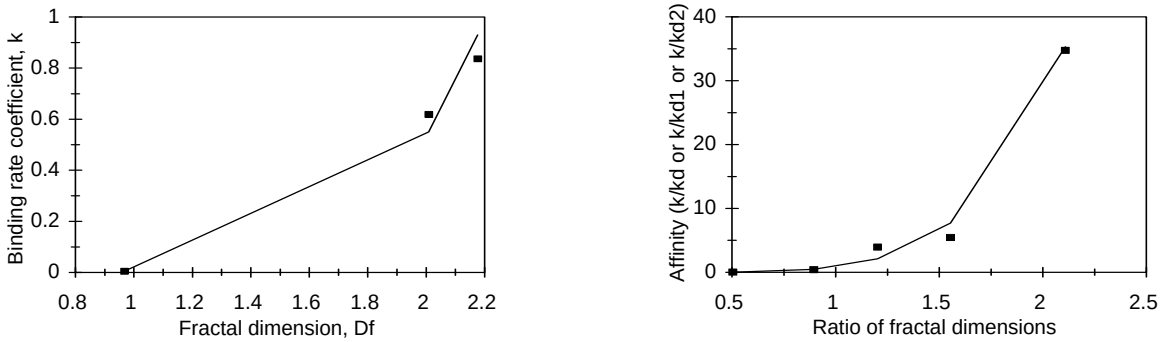


a) b)

**Fig. 13.** (a) Increase in the binding rate coefficient, k with an increase in the fractal dimension, $D_f$; (b) Increase in the affinity, K with an increase in the ratio of fractal dimension present in the binding phase to that present in the dissociation phase.

For the data presented in Tables 4a and 4b, Fig.13b shows the increase in the affinity, K value with an increase in the corresponding ratio of the binding rate coefficient to the dissociation rate coefficient. The affinity, K is given by:

$$K = (0.8446 \pm 0.4479)\,(\text{ratio of the fractal dimension present in the binding phase to that in the dissociation phase})^{5.00 \pm 0.3887} \quad (7b)$$

The fit is very good, considering that two different data sets are used and plotted together. The affinity, K is very sensitive to the ratio of fractal dimensions present in the binding phase and in the dissociation phases as noted by the fifth order of dependence exhibited.

## 4. Conclusions

A fractal analysis is presented for (a) the binding of different concentrations of mouse monoclonal anti-rabbit IgG in solution to rabbit patterned cells using a diffraction-based sandwich immunoassay [2], (b) the binding and hybridization of DNA using a double-wavelength technique for surface plasmon resonance measurements [3], (c) the binding and dissociation of different concentrations of GSH-(Glutathione)-MPC (monolayer protected clusters) in solution to polyclonal antibody plus Protein A immobilized on a quartz crystal microbalance (QCM) [4], and (d) the binding and dissociation of substance P (neuropeptide) (SP) in solution to quencher-labeled mAb (monoclonal antibody)) SP31 using the SPIT-FRI (solid phase immobilized tripod for fluorescent renewable immunoassay) procedure [5]. The fractal analysis is used to provide better insights into the analyte-receptor interactions occurring on these novel types of sensing surfaces or modifications of previously employed sensing surfaces. The fractal analysis helps relate the binding (and the dissociation) rate coefficients with the degree of heterogeneity that exists on these sensing surfaces.

The fractal analysis provides a quantitative indication of the state of disorder (fractal dimension) and the binding (and dissociation) rate coefficients on the sensor chip surface. Both types of examples are given wherein either a single- or a dual-fractal analysis was used. The dual-fractal analysis was used only when the single-fractal analysis did not provide an adequate fit. This was done by the regression analysis provided by Corel Quattro Pro 8.0 [20].

In accordance with the prefactor analysis or fractal aggregates [29], quantitative (predictive) expressions are developed for (a) the binding rate coefficient, $k_1$ as a function of the fractal dimension, $D_{f1}$ for the binding of 50-250 ng/mL anti-rabbit IgG concentration in solution to rabbit IgG patterned cells [2], (b) the binding rate coefficient, $k_2$ as a function of the anti-rabbit IgG concentration in solution [2], (c) the ratio of the binding rate coefficients, $k_2/k_1$ as a function of the ratio of fractal dimensions, $D_{f2}/D_{f1}$ [2] and (d) the binding rate coefficient, $k_1$ as a function of the fractal dimension, $D_{f1}$ for the binding (hybridization) of G-HCV in solution to G-HCV immobilized on the spot surface and for the selective hybridization of G-HCV-c and $T_2$–HCV-c in solution to complementary sequences immobilized at different spot surfaces [3].

Predictive-type relations are also developed for (a) the binding rate coefficients, $k_1$ and $k_2$ for GSH (glutathione)-MPC (monolayer protected clusters) in solution to polyclonal anti-GSH + protein A immobilized on a quartz crystal microbalance (QCM) as a function of the GSH-MPC concentration in solution [4], (b) the binding rate coefficient, $k_1$ as a function of the fractal dimension, $D_{f1}$ for the binding of substance P (neuropeptide) (SP) in solution to quencher-labeled mAb (monoclonal antibody) SP231 using the SPIT-FRI procedure [5], and finally (c) the affinity, K (ratio of binding to dissociation rate coefficients) as a function of the ratio of fractal dimensions present in the binding and in the dissociation phase.

In general, the binding rate coefficient is quite sensitive to the fractal dimension or the degree of heterogeneity that exists on the surface as noted by the order of dependence exhibited on the fractal dimension, $D_f$. As indicated in earlier manuscripts, the fractal dimension is not a classical independent variable such as analyte (antigen, antibody, or other biological molecule) concentration in solution. Nevertheless, the high orders mentioned above for the dependence of the binding rate coefficient on the fractal dimension of these novel biosensor methods or modifications of existing biosensors being employed emphasize the importance of the extent of heterogeneity on these sensing surfaces and their impact on the binding rate coefficient. This would also significantly impact biosensor performance parameters such as sensitivity, regeneration, stability, and response time. Hopefully, the emphasis on the surface of these novel biosensors would further facilitate in help improving these biosensors and further help in extending their applicability to other areas of usage.

## References

[1]. C. P. Quinn, V. A. Semenova, C. M. Elie, S. Romero-Steiner, C. Greene, H. Li, K. Stamey, E. Steward-Clark, D. S. Schmidt, *Emerging Infectious Diseases*, Vol. 8, 2002, pp. 1103-1110.

[2]. J. B. Goh, P. L. Tam, R. W. Loo, M. C. Goh, A quantitative diffraction-based sandwich immunoassay. Analytical Biochemistry, Vol. 313, 2003, pp. 262-266.

[3]. A. Zybin, C. Granwald, V. M. Mirsky, J. Kuhlmann, J., O. S. Wolfbeis, K. Niemax, (2005). Double-wavelength technique for surface plasmon resonance measurements: basic concept and applications for single sensors and two-dimensional sensor arrays. Analytical Chemistry, Vol. 77, No. 8, 2005, pp. 2393-2399.

[4]. A. E. Gerdon, D. W. Wright, D. E. Cliffel, Quartz crystal microbalance: detection of glutathione-protected nanoclusters using antibody recognition. Analytical Chemistry, Vol. 77, No. 2, 2005, pp. 304-310.

[5]. H. Volland, L. M. Neuberger, E. Schultz, J. Grassi, F. Perrant, C. Creminion, (2005). Solid-phase immobilized tripod for fluorescent renewable immunoassay. A concept for continuous monitoring of an immunoassay. Analytical Chemistry, Vol. 77, 2005, 1896-1904.

[6]. S. Havlin, Molecular Diffusion and Reaction. In: Avnir, D. (Ed.), The Fractal Approach to Heterogeneous Chemistry: Surfaces, Colloids, Polymers. Wiley, New York, 1989, pp. 251-269.

[7]. A. Sadana, A kinetic study of analyte-receptor binding and dissociation, and dissociation alone for biosensor applications: a fractal analysis. Analytical Biochemistry, Vol. 291, 2001, pp. 34-47.

[8]. A. Ramakrishnan, A. Sadana, A single-fractal analysis of cellular analyte- receptor binding kinetics utilizing biosensors. Biosystems, Vol. 59, 2001, pp. 35-51.

[9]. S. J. Thomson, G. Webb, Heterogeneous Catalysis, Wiley, New York, 1968, p.23.
[10]. W. Rudzinski, L. Latter, J. Zajac, J., E. Wofram, E. J. Paszli, Ideal adsorption from binary liquid mixtures on a heterogeneous solid surface: Equations for excess isotherms and heats of immersion. Journal of Colloid & Interface Science, Vol. 96, 1983, pp. 339-359.
[11]. A. Dabrowski, M. Jaroniec, Effects of surface heterogeneities in adsorption from binary liquid mixtures. III. Analysis of experimental data using Langmuir-Freundlich type equations. Journal of Colloid & Interface Science, Vol. 73, 1979, pp. 475-482.
[12]. J. Oscik, A. Dabrowski, M. Jaroniec, M., W. Rudzinski, Effects of surface heterogeneity in adsorption from binary liquid mixtures. I. Adsorption from ideal solutions. Journal of Colloid & Interface Science, Vol. 56, 1976, pp. 403-412.
[13]. M. Jaroniec, A. Derylo, Simple relationships for predicting multisolute adsorption from dilute aqueous solutions. Chemical Engineering Science, Vol. 36, 1981, pp. 1017-1019.
[14]. C. K. Lee, S. L. Lee, Multi-fractal scaling analysis of reactions over fractal surfaces. Surface Science, Vol. 325, 1995, pp. 294-310.
[15]. F. Nakajima, Y. Hirakawa, T. Kaneta, T. Imasaka, Diffractive optical chemical sensor based on light absorption. Analytical Chemistry, Vol. 71, 1999, pp. 2262-2265.
[16]. G. A. Mines, B. C. Tzeng, K. J. Stevenson, J. L. Li, J. T. Hupp, Microporous supramolecular coordination compounds as chemosensory photonic lattices. Angew Chemistry International Edition Vol. 41, 2002, pp. 154-157
[17]. Y. G.Tsay, C. I. Lin, J. Lee, E. K. Gustafson, R. Appelqvist, P. Magginetti, R. Norton, N. Teng, D. Charlton, Optical biosensor assay (OBATM). Clinical Chemistry, Vol. 37, No. 9, 1991, pp. 1502-1505.
[18]. P. M. St. John, R. Davis, N. Cady, J. Czaka, C. A. Batt, H. G. Craighead, Diffraction-based cell detection using a microcontact printed antibody grating. Analytical Chemistry, Vol. 70, 1998, pp. 1108-1111.
[19]. F. Morhard, J. Pipper, R. Dahint, M. Grunze, Immobilization of antibodies in micropatterns for cell detection by optical diffraction. Sensors & Actuators B Chemical, Vol. 70, 2000, pp. 232-242.
[20]. Corel Quattro Pro 8.0, 1997, Corel Corporation, Ottawa, Canada.
[21]. B. Leidberg, C. Nylander, I. Lundstrom, Biosensing with surface plasmon resonance – how it all began. Biosensors & Bioelectronics, Vol. 10, 1995, i-ix.
[22]. G. T. Hermanson, *Bioconjugate Technique*, 1995, Academic Press, San Diego.
[23]. W. M. Albers, I. Vikholm, T. Viitala, T., J. Peltonen, Handbook of Surfaces and Materials, Vol. 5, 2001, Academic Press, San Diego, pp. 1-31.
[24]. N. Wrobel, M. Schinkinger, V. M. Mirsky, A novel ultraviolet assay for testing side reactions of carbodiimides. Analytical Biochemistry, Vol. 305, 2002, pp. 135-138.
[25]. S. A. Zynio, A. V. Samoylov, E. R. Surovtseva, V. M. Mirsky, Y. M. Shirshov, Bimetallic layers increase sensitivity of affinity sensors based on surface plasmon resonance. Sensors, Vol. 2, 2002, pp. 62-68.
[26]. E. Alieva, V. N. Konopsky, Biosensor based on surface plasmon resonance interferometry independent on variations of liquid's refractive index. Sensors & Actuators B Chemical, Vol. 99, 2004, pp. 90-97.
[27]. N. Wrobel, W. Deininger, P. Hegemann, V.M. Mirsky, Covalent immobilization of oligonucleotides on electrodes. Colloids and Surfaces B: Biointerfaces, Vol. 32, 2003, 32, pp. 157-162.
[28]. H. Volland, C. Creminon, L. M. Neuberger, J. Grassi, French patent, 0214959, 2002.
[29]. C.M. Sorenson, G.C. and Roberts, (1997). The prefactor of fractal aggregates. Journal of Colloid and Interface Science, Vol. 186, 1997, 447-452.

---

# Guide for Contributors

## Aims and Scope

*Sensors & Transducers Journal (ISSN 1726- 5479)* provides an advanced forum for the science and technology of physical, chemical sensors and biosensors. It publishes state-of-the-art reviews, regular research and application specific papers, short notes, letters to Editor and sensors related books reviews as well as academic, practical and commercial information of interest to its readership. Because it is an open access, peer review international journal, papers rapidly published in *Sensors & Transducers Journal* will receive a very high publicity. The journal is published monthly as twelve issues per annual by International Frequency Association (IFSA). In additional, some special sponsored and conference issues published annually.

## Topics Covered

Contributions are invited on all aspects of research, development and application of the science and technology of sensors, transducers and sensor instrumentations. Topics include, but are not restricted to:

- Physical, chemical and biosensors;
- Digital, frequency, period, duty-cycle, time interval, PWM, pulse number output sensors and transducers;
- Theory, principles, effects, design, standardization and modeling;
- Smart sensors and systems;
- Sensor instrumentation;
- Virtual instruments;
- Sensors interfaces, buses and networks;
- Signal processing;
- Frequency (period, duty-cycle)-to-digital converters, ADC;
- Technologies and materials;
- Nanosensors;
- Microsystems;
- Applications.

## Submission of papers

Articles should be written in English. Authors are invited to submit by e-mail editor@sensorsportal.com 4-12 pages article (including abstract, illustrations (color or grayscale), photos and references) in both: MS Word (doc) and Acrobat (pdf) formats. Detailed preparation instructions, paper example and template of manuscript are available from the journal's webpage: http://www.sensorsportal.com/HTML/DIGEST/Submition.htm Authors must follow the instructions strictly when submitting their manuscripts.

## Advertising Information

Advertising orders and enquires may be sent to sales@sensorsportal.com Please download also our media kit: http://www.sensorsportal.com/DOWNLOADS/Media_Kit_2007.PDF